nanomaterials

MDPI

Article

RETRACTED: Capacitive Behavior of Aqueous Electrical Double Layer Based on Dipole Dimer Water Model

Songming Yang [1,2], Youer Deng [1] and Shiqi Zhou [1,*]

[1] School of Physics and Electronics, Central South University, Changsha 410083, China
[2] Zhili College, Tsinghua University, Beijing 100084, China
* Correspondence: chixiayzsq@163.com

Abstract: The aim of the present paper is to investigate the possibility of using the dipole dimer as water model in describing the electrical double layer capacitor capacitance behaviors. Several points are confirmed. First, the use of the dipole dimer water model enables several experimental phenomena of aqueous electrical double layer capacitance to be achievable: suppress the differential capacitance values gravely overestimated by the hard sphere water model and continuum medium water model, respectively; reproduce the negative correlation effect between the differential capacitance and temperature, insensitivity of the differential capacitance to bulk electrolyte concentration, and camel–shaped capacitance–voltage curves; and more quantitatively describe the camel peak position of the capacitance–voltage curve and its dependence on the counter-ion size. Second, we fully illustrate that the electric dipole plays an irreplaceable role in reproducing the above experimentally confirmed capacitance behaviors and the previous hard sphere water model without considering the electric dipole is simply not competent. The novelty of the paper is that it shows the potential of the dipole dimer water model in helping reproduce experimentally verified aqueous electric double layer capacitance behaviors. One can expect to realize this potential by properly selecting parameters such as the dimer site size, neutral interaction, residual dielectric constant, etc.

Keywords: aqueous electrolyte; electric dipole; electrical double layer capacitor; differential capacitance; nanoconfinement

check for updates

Citation: Yang, S.; Deng, Y.; Zhou, S. RETRACTED: Capacitive Behavior of Aqueous Electrical Double Layer Based on Dipole Dimer Water Model. *Nanomaterials* **2023**, *13*, 16. https://doi.org/10.3390/nano13010016

Academic Editor: Fabrizio Pirri

Received: 15 November 2022
Revised: 24 November 2022
Accepted: 27 November 2022
Published: 20 December 2022
Retracted: 24 December 2024

Copyright: © 2022 by the authors. Licensee MDPI, Basel, Switzerland. This article is an open access article distributed under the terms and conditions of the Creative Commons Attribution (CC BY) license (https://creativecommons.org/licenses/by/4.0/).

1. Introduction

The electrical double layer capacitor (EDLC) is an energy-storage device that stores electrical energy physically through charge separation at the electrode–electrolyte interface without involving faradaic reaction. Such surface storage causes only minor, if any, volume change of the electrode during operation, resulting in a long cycle life (>10^6 charge–discharge cycles), as well as a fast charge rate, similar to discharge; the characteristics very distinct from batteries also include a wide temperature range of operation and environmental friendliness [1–3]. To address the EDLC low energy density, the hybrid electrochemical capacitor (HEC) [4,5] was invented, which employs a battery electrode, created from a variety of redox-active electrolytes either dissolved in the electrolyte or adsorbed/immobilized in nanoporous electrodes and reversibly harnessing redox reactions with a negative electrical double-layer (EDL) capacitive electrode storing charge. As one of the important components of the EDLCs, electrode materials [6,7] have produced a lot of progress, effectively improving the EDLC performance (such as specific capacitance, energy storage density, power density, voltage stability window, etc.). At present, the electrolytes suitable for the EDLC include organic-based ionic liquids and aqueous electrolytes. Although aqueous electrolytes have disadvantages such as narrow electrochemical windows of 1.23 V due to the hydrogen/oxygen evolution reactions, they have benefits of high ionic conductivity, non-flammability, and low manufacture costs in comparison with their organic counterparts. In fact, the limitation of the narrow electrochemical window

This paper has been retracted. A retraction notice was published on 24 December 2024 in *Nanomaterials* **2025**, *15*, 1.
https://doi.org/10.3390/nano15010001

RETRACTED

can be overcome in highly concentrated aqueous electrolytes, also known as water-in-salt (WiS) electrolytes [8–13], which have been shown to significantly widen the electrochemical stability window to over 3.0 V, via interface modification [14,15], or the development of chemically stable, high surface area carbon structures [16–18]. As a result, aqueous electrolytes are still popular in the study of EDLCs [19–28].

In Molecular Dynamics and Monte Carlo simulations [29–49] of the EDLCs, realistic force fields can be used; for example, solvent water is modeled by popular water models such as the SPC/E model. Ions can have very complex structures, such as organic ionic liquids. As a result, the influences of molecular details on the EDLC capacitive behaviors can be revealed. In theoretical studies, simpler coarse-grained models are used, but essential features can be captured. Usually, the aqueous electrolyte solution is modeled by so-called primitive model (PM) [20,22,50–52], in which a water solvent is considered as a structureless continuum and shows its existence only through a high dielectric constant completely neglecting its hard core; some researches [53–60] pick up the hard core missed in the PM and use an appropriately high dielectric constant to reflect the electric dipole moment of the water molecule (such a model is called the solvent primitive model abbreviated as SPM). There are studies [61,62] that consider a semi-primitive model where the solvent is represented by hard spheres with a Yukawa attraction and a dielectric permittivity is also introduced to reflect the electrostatic shielding effect of water molecules; in a very recent study [63], one Lennard–Jones (LJ) sphere with a higher energy parameter is used to model the water molecule to reflect its strong polarity, both the LJ energy and size parameters are determined by reproducing the two experimentally measured a and b parameters in the van der Waals equation of the state of water. More advanced models (the so-called "civilized" model) have been proposed, where both the polar nature and hard core of the solvent molecule are explicitly considered at the same time, by a dipole hard sphere (hard sphere carrying a point dipole at its center) [64–66] or dipole dimer hard sphere with positive and negative polarized charges residing in the centers of the two constituent spheres [67]. The dipole dimer hard sphere model of water is less applied in conjunction with capacitive behavior investigation of the EDLC in aqueous electrolyte solution because of the convergence problem [67]. In the literature [67], it is illustrated that the classical density functional theory (CDFT) converges only for relatively small electrode potentials. However, the dipole dimer hard sphere model is more realistic than the dipole hard sphere because the former takes into account the multicore of the water molecule.

The aim of the present work is to reproduce the experimentally observed capacitive behaviors of the aqueous EDLC with help from the classical density functional theory (CDFT) in which the water is modeled by a more realistic dipole dimer hard sphere model and the salt ions are approximated by charged hard spheres as in the PM. Compared with a large number of reports on the aqueous EDLC capacitance behaviors based on the PM [20,22,50–52,68] and SPM [53–60], the report of capacitance behaviors of the EDLC based on the dipole dimer hard sphere model for water is almost blank (instead of the EDLC capacitance behaviors, the literature [67] only reports the electrical double layer structure). So, the present report is necessary and urgent.

The structure of the present paper is as follows. In Section 2, the models for solvent water and salt ions are detailed; the terms in the free energy functional describing the internal inter-particle interactions are expounded, and the procedure for numerically solving the CDFT equation is explained. In Section 3, we perform the CDFT calculations to find the possible changes caused by the replacement of the solvent hard sphere model by the dipole dimer hard sphere model and compare with the experimental results. Finally, in Section 4, we summarize the present findings.

2. Model and Method

The neutral cohesive interactions between fluid phase particles and those between the fluid phase particles and constitute particles of the solid surface are shown to cause significant changes in the density profiles, which necessarily produce a variation of the

RETRACTED

capacitive behaviors [61,63]; they are not considered in the present study because our main goal is to study the changes caused by the explicit consideration of the hard core and electric dipole of the water solvent. So, the inorganic salt ions are modeled by appropriately charged hard spheres and the water molecule is approximated as a dimer consisting of two hard sphere sites (representing the hydrogen atom and oxygen atom, respectively) tangentially bonded together and rotating freely on each other's surfaces. The diameters of hydrogen and oxygen sites and the polarized charges on them are denoted by d_H, d_O, and q_H and q_O, respectively. Similarly, the diameters and charges of cation and anion are denoted by d_+, d_-, and q_+ and q_-, respectively. Throughout the paper, $q_+ = -q_- = e$ ($e = 1.6 \times 10^{-19}C$ is elementary charge strength). Throughout all calculations, if not otherwise declared, the thermodynamic temperature T is fixed at 298.15 K; $q_H = -q_O = 0.203947e$ and $d_H = d_O = 1.9$Å, so the electric dipole moment on the model water molecule is $p_e = 6.2 \times 10^{-30}mC \approx 1.86D$, very close to the electric dipole moment of real water molecule; $d_+ = d_- = 3.2$Å and $\varepsilon_r = 6.0$. In principle, because we have explicitly considered the electric dipole moment of water, the electrostatic interaction in the solution should be the same as that in vacuum, i.e., the relative dielectric constant of the medium should be one. However, in real systems, ions and water molecules will undergo displacement polarization and orientation polarization in a strong electric field; therefore, the electrostatic interaction will be weakened. In theory, we consider this polarization effect by setting the relative dielectric constant at a value appropriately greater than 1. We calculate the water molar concentration c_w by referring to the aqueous potassium chloride solution and density and molecular weight of potassium chloride and water at room temperature, assuming that the volume of the potassium chloride remains unchanged after it is dissolved in water:

$$c_w = (1000 - 74.5c_{1:1}/1.98)/18. \quad (1)$$

where $c_{1:1}$ is molar concentration of +1:−1 type inorganic salt. The electrode is modeled by a slit-shaped pore consisting of two surfaces in parallel; in order to highlight the effect caused by the explicit consideration of the hard core and electric dipole of the water molecule as much as possible, we will not consider the van der Waals interactions between the surface atoms and fluid particles (cation, anion, and water molecule) for the time being; instead, we treat the surface as a hard wall.

We employ the MISAF theory [69] to treat the bonding functional forming the dimer model water molecule. The advantage of the MISAF theory is that it can ensure that various sites on the heteronuclear chain molecule meet the overall stoichiometry provided by the molecular structure. Specifically, the present dipolar dimer hard sphere model of the water molecule can be regarded as a heteronuclear chain; when the electrical double layer (EDL) in the electrode pore reaches equilibrium, the total number of the hydrogen site and oxygen site should be equal; if they are indeed equal, the situation are called to satisfy the overall site stoichiometry. However, the overall stoichiometry will be seriously violated if the interfacial statistical associating fluid theory is employed instead, especially when the electrode pore is extremely narrow. The satisfaction of the overall stoichiometry further increases the difficulty of numerical solution convergence. For this reason, (i): Start the calculation from the zero-surface charge density and use the density distribution output of the previous charge density as input of the next charge density calculation; the difference between the two charge densities is very small, for example 8×10^{-5} C/m^2. In this way, the surface potential can be calculated up to 5 V, which causes it to be possible to calculate the differential capacitance–voltage curves over a wide voltage range. (ii) The nonlinear equations resulting from the discretized CDFT equation are solved by the Newton GMRES algorithm as implemented in the public-domain nonlinear Krylov solver NITSOL [70]. The examples [60,71–74] show that the GMRES algorithm is often effective in dealing with electrostatic systems.

The advantage of the CDFT is that the functionals corresponding to various types of inter-molecular interactions can be approximated and tested separately. Based on this, on the basis of the MISAF theory, by adding the fundamental measure functional for the hard

RETRACTED

sphere interaction, the mean field approximation for the long-range electrostatic interaction, and the second-order functional expansion for the coupling of electrostatic and hard sphere interactions, one can determine the so-called excess free energy functional of this model, and the whole free energy functional can be determined by further adding the well-known ideal gas functional.

Given the system temperature T, bulk electrolyte mole concentration $c_{1:1}$, and electrode surface charge density σ, the CDFT equation is solved; then, the corresponding electrostatic potential distribution $\psi(z)$ (including the electrode potential U) and particle density distributions $\rho_\alpha(z)$ ($\alpha = +, -, w$ represent cation, anion, and water molecule, respectively) can be obtained. The differential capacitance C_d, an experimentally accessible quantity reflecting some of the EDL properties, is defined via:

$$C_d = \partial\sigma/\partial U \tag{2}$$

3. Results and Discussion

We mainly investigate how the differential capacitance C_d responds to changes of the system parameters under the condition of explicit consideration of the hard core and electric dipole of the water molecule, analyze the microscopic origin of this response, and compare the situation with that of the theoretical and/or simulation calculations based on the PM and SPM, as well as experiments, so as to judge the rationality of introducing the dipole dimer water model into the EDLC. Moreover, we analyze the individual effect of electric dipole and hard core of water molecule.

First, we discuss the order of magnitude of C_d and the shapes of C_d–U curves. Both the simulation and theory calculations using the PM generally overestimate the value of C_d to two orders of magnitude. For example, in the literature [20], adopting the dielectric constant of bulk water as that in the cylindrical pore, the calculated C_d is generally around 3 F/m^2; the decreasing of the counter-ion size and/or increasing of the counter-ion electric valence will further increase the C_d value. However, in the dipole dimer hard sphere model of water, for the 1:1 type electrolyte of equal size, the C_d is generally around 0.03 F/m^2, as illustrated in the present Figure 1. The MD simulation using the SPC/E model of water provides the C_d around 0.05 F/m^2 [75], with which the present results are far more consistent than those based on the PM. Although there is still a difference between the capacitance value based on the dipole dimer water model and that based on the SPC/E model, the difference is far less than that involving the PM model. Considering the neutral interactions between ions and electrode are completely ignored, the other parameters of the present ions and electrode are different from those in the literature [75], the parameters of the dipole dimer water model are also only reasonable estimates, and we can believe that this difference can be greatly reduced by carefully selecting the relevant parameters. It is gratifying that although the dipole dimer model is much simpler than the SPC/E model, it provides quite consistent results with that delivered by the latter.

As for the shapes of the C_d–U curves, the molecular simulation and theoretical calculation using PM generally show [20,76] that the aqueous EDLC C_d–U curves change from a camel-shaped to a bell-shaped curve with an increase in the bulk concentration; the transition bulk concentration is mostly and at least at the lower limit of the high concentration, for example, around 2.5 M for the PM aqueous EDLCs. The transition between the camel- and bell-shaped curves also occurs for ionic liquids and molten salt EDLCs [77,78]. However, by using more realistic water simulation, we always obtain camel-shaped curves for aqueous EDLC even if the bulk concentration is increased to 6 M, as shown in Figure 1. In the experiment, the bell-shaped curves have also never been observed for the aqueous EDLC. Therefore, the dipole dimer water model can provide a more practical capacitance–voltage curve shape.

RETRACTED

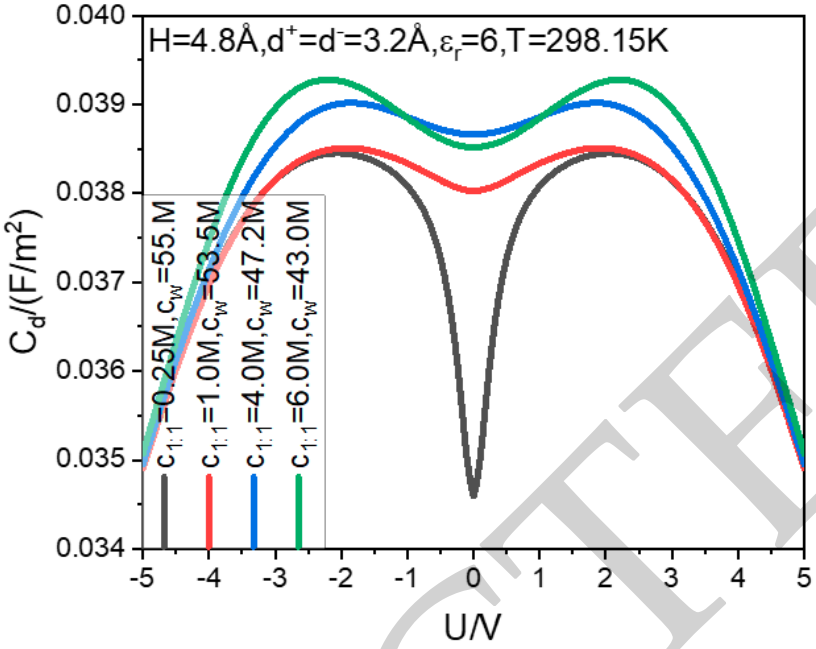


Figure 1. Correlation between the bulk electrolyte concentrations and differential capacitance–voltage curves.

The influence of the bulk concentration on the capacitance is plotted in Figure 2. Except for very low voltage, the influence is actually very small; the span of the bulk concentration reaches five orders of magnitude, while the change of capacitance is only 0.3 μF/cm^2. The experimental data of the completely same system do not exist, but there are experimental curves for the capacitance–bulk concentrations of similar systems reported. In the literature [79], the C_d of the planar electrode EDLC in an aqueous sodium chloride solution is measured over a wide range of concentration; it is found that the C_d remains still in the same order of magnitude over such a wide concentration range from 10^{-5} M to 1 M. The present dipole dimer model calculations are obviously consistent with the experiments in terms of the capacitance effect of the bulk concentration.

The temperature effect of the capacitance–voltage curve is plotted in Figure 3a. With an increase in temperature, the curve moves down as a whole, which indicates that, in the temperature range from 288.15 K to 358.15 K, the capacitance is inversely related to the temperature at all voltages. In the literature [80], the electrochemical impedance spectroscopy is used to measure the double layer capacitance of the polycrystalline Pt–aqueous $HClO_4$ solutions interface; therein, it is illustrated that the capacitance decreases with the solution temperature increasing. It is considered [80] that the inverse correlation is mainly due to the dropping of the dielectric constant at elevated temperatures, which leads to such an effect. In the present work, although the redundant permittivity is fixed at 6.0, the water model we use takes into account the electric dipole moment of the real water molecule, so the calculated equilibrium density distributions must reflect the influence of the water molecule electric dipole on the electrostatic shielding and certainly also take into account the weakening of the electrostatic shielding or, in other words, the dropping of the dielectric constant, caused by the rise of temperature. Consequently, the present dipole dimer hard sphere model calculations should be consistent with the experiment measures, as it is. It should be pointed out that the simulation [81] using PM discloses a low temperature anomaly in the double layer capacitance, i.e., at low temperatures, the capacitance in dissolved electrolytes decreases with decreasing temperatures; in the same work, it is also shown that at higher temperatures the experimentally confirmed C_d–T negative correlation is still recovered. Considering that the PM C_d–T positive correlation behavior is similar to the capacitance behavior of the molten salt double layer and the molten salt is solvent free, we can infer that the positive C_d–T correlation at lower temperatures and in the PM

RETRACTED

aqueous electrolyte solution is artificial and caused by ignoring the hard core of the water molecule and simply replacing the electric dipole with a dielectric constant. To show the effect of explicit consideration of the water molecule electric dipole moment and hard core in enabling the realization of the negative correlation C_d–T, we repeat the calculations in Figure 3a with the polarized charges on hydrogen and oxygen atoms switched off and the water mole concentration still calculated by Equation (1); the relevant results are exhibited in Figure 3b. In Figure 3c, we present the calculations for the C_d–T curves with the PM, i.e., both the hard core and electric dipole of the water molecule are omitted completely. Considering that very small electrode pores are being under consideration and the electric dipole is not considered in the calculations of Figure 3b,c, the relative dielectric constant in the pore is set as $\varepsilon_r = 10$ and in the bulk it is still set as $\varepsilon_{br} = 78.5$. The molecular dynamics simulations show that the perpendicular component of the water dielectric constant drastically decreases in narrow pores [82,83] compared with the bulk water dielectric constant; so, we choose a small value for the dielectric constant of water in the pore. From the information provided in Figure 3, we can produce four analyses. First, the three water models can provide the inverse correlation effect between C_d and T, but the dimer hard sphere model and PM model provide an extremely weak inverse correlation effect, which is inconsistent with the experiment [80]; while the dipole dimer hard sphere model provides a more obvious inverse correlation effect, which is more consistent with the experimental measure [80]. Second, the explicit consideration of the water molecule hard core without the electric dipole causes an unexpected phenomenon: raising capacitance, rather than reducing the seriously overestimated capacitance caused by the adoption of PM; the overestimation also can be caused by using the solvent hard sphere model to represent the water molecule hard core [58]. This shows that the specific shape of the hard core, whether it is a single hard sphere or a dimer hard sphere, does not change the qualitative behavior of the capacitance curve. Third, it is shown [58] that if the electric dipole of the water molecule is not considered, the hard core alone induces another trend contrary to the experiment: induces the transition between camel- and bell-shaped capacitance–voltage curves. Finally, as can be seen from Figure 3, three different water models provide different camel peak positions; the dipole dimer hard sphere model provides the position of about 2.0 V, the dimer hard sphere model provides 0.7 V, and the PM provides 0.625 V. Furthermore, the recent simulation and CDFT calculation [20] show that, in the case of extremely small electrode pores (equivalent to the pore size in this paper), the camel peak position is approximately less than 0.2 V. From the c sub-graph of Figure 4 in the literature [80], we can find that even when the voltage reaches 1.0 V, there is still no sign of the camel peak; from the curve trend, the camel peak position may be more than 1.5 V. In a word, the electric dipole dimer hard sphere water model provides the most reliable camel peak position quantitatively compared with the experiment, followed by the dimer hard sphere water model without considering the electric dipole, and finally the continuum media water model.

As for why the electric dipole dimer water model provides the most accurate camel peak position, we think it is because, in the continuum media model, the solvent molecules do not compete with ions for limited electrode pore space, so only a small voltage is required to achieve the maximum adsorption capacity of ions and maintain it. In the dimer hard sphere model, the solvent molecules in the form of dimer hard sphere will also be adsorbed in the pore and compete for the pore space with the adsorption of ions. To drive the solvent out of the pore, the voltage must be increased, so as to expand the difference between the driving forces for ions and solvent entering the electrode pore. In the case of the dipole dimer water model, although the water molecule is still neutral as a whole, the electrostatic interaction between the water molecule and the charged electrode is not zero due to the existence of the electric dipole. Through the automatic adjustment of the direction of the electric dipole moment, the electrostatic interaction between the electric dipole and the charged electrode is attractive. Therefore, the consideration of the electric dipole will certainly increase the driving force for water adsorption into the pore. In order

RETRACTED

to expel it, the electrode voltage must be increased, so as to cause the camel peak to move outward, as it is.

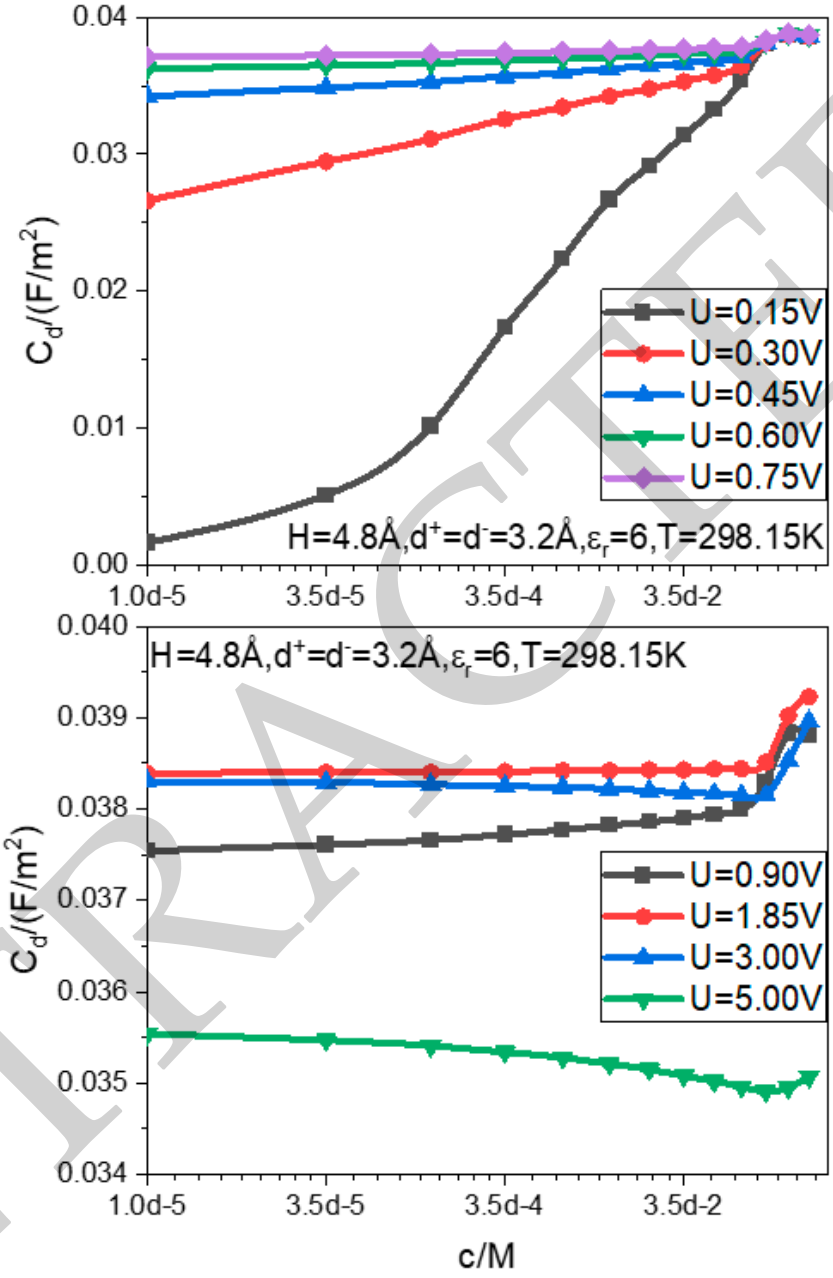


Figure 2. Function relation between the differential capacitance C_d and bulk electrolyte concentration c at different electrode potentials U.

To summarize, considering the electric dipole on the basis of the water hard core can cause the capacitance behaviors to be more consistent with the experiments in several aspects, such as the location of the camel peak, intensity of the temperature effect, suppressing the capacitance value badly overestimated by the PM, capacitance effect of bulk concentration, and the shape of capacitance–voltage curves. So, one can conclude that the electric dipole of the water molecule plays a crucial and important role in the model of EDLC capacitance behaviors; it is not advisable to simply use a higher dielectric constant to average the electric dipole effect.

RETRACTED

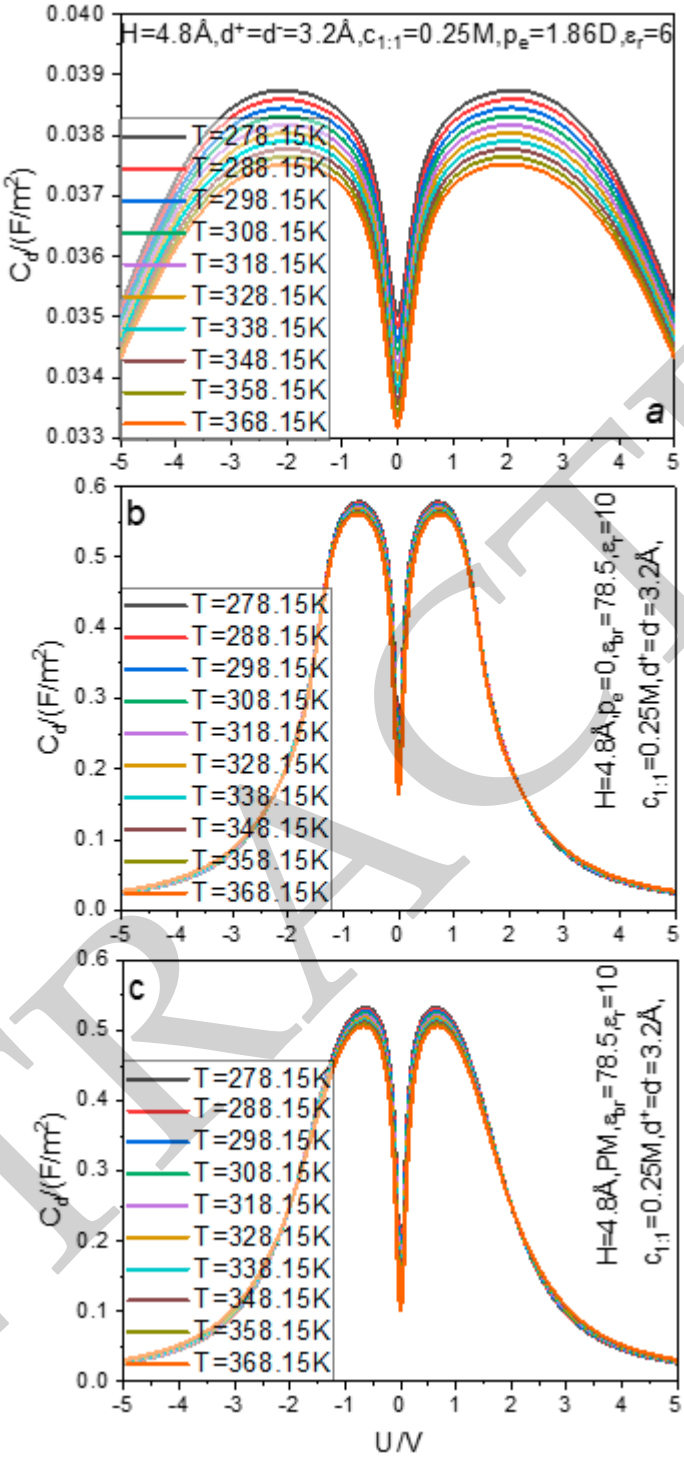


Figure 3. Correlation between the temperature *T* and differential capacitance–voltage curves (**a**–**c**).

In Figure 4, the capacitance–voltage curves for different ion sizes are plotted together to compare the effects of the ion size in the dipole dimer hard sphere model of water solvent. By comparing the present Figure 4 with Figure 6 in the literature [84], one can draw a conclusion that the PM can obtain qualitatively consistent results as the dipole dimer hard sphere model from a perspective of the capacitance effects of ion size. First, in both models, the capacitance decreases with the counter-ion size and is relatively stable relative to change of the co-ion size; second, both models predict the camel peak position moves to high voltage with the counter-ion size decreasing. As for why the peak position

RETRACTED

increases with the decrease in the counter-ion size, we speculate that the decrease in the counter-ion size causes more counter-ions to be adsorbed near the electrode (the increase in C_d is a manifestation), so the electrostatic repulsion in the EDL is strong. In order to pack more counter-ions into the pore, the voltage must be increased.

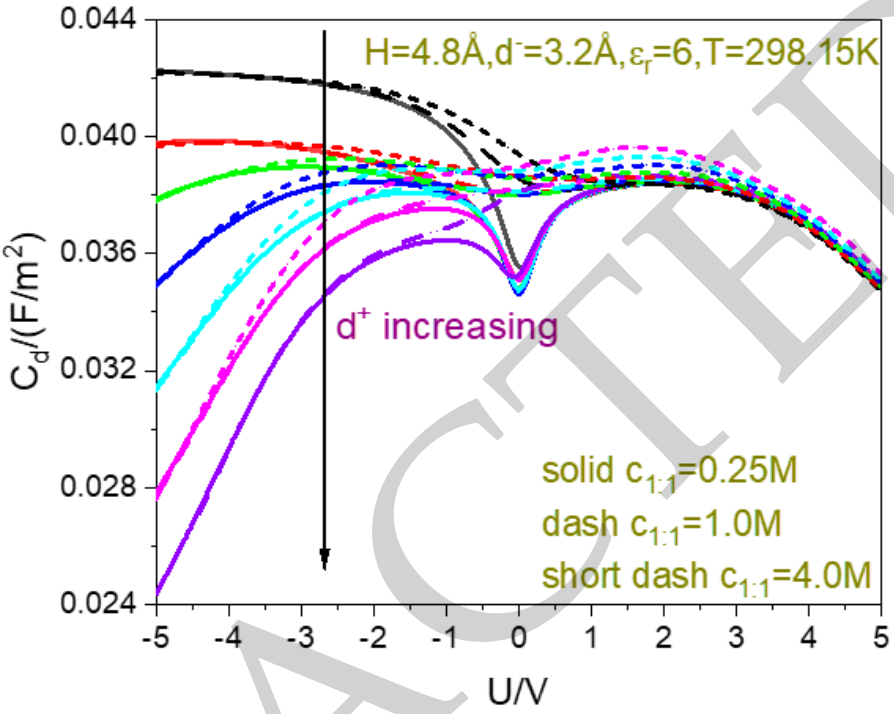


Figure 4. Correlation between the counter- and co-ion sizes and differential capacitance–voltage curves. The cation diameter in Å changes from 2, 2.4, 2.8, 3.2, 3.6, 4.0, to 4.4.

4. Summary

In the present paper, the capacitive behaviors of an aqueous electrolyte solution EDLC are investigated by theoretical calculations based on the CDFT incorporating electric dipole and hard core of the solvent water molecule. By comparing the present capacitance curves with those from the PM based on the continuum media water model and SPM based on the hard sphere water model, we observe that the present capacitance behaviors are different from those from the continuum media and hard sphere water models and more consistent with the relevant experimental results. Specifically, given reasonable model parameters, the dipole dimer hard sphere model: (i) can restrain the value of differential capacitance C_d seriously overestimated by both the continuum media and hard sphere water models, respectively; (ii) predicts that the C_d–voltage curve is always camel-shaped; (iii) can describe the inverse correlation between C_d and temperature; and (iv) can create possible the relative stability of C_d value in a wide range of aqueous electrolyte bulk concentrations; and (v) describes the camel peak positions of the capacitance–voltage curves more accurately than the other two water models and its inverse correlation with the counter-ion size. However, the continuum media and hard sphere water models fail in these four aspects or cannot reflect the experimental results well. The importance of the water electric dipole lies in that its explicit consideration is essential to describe the above aspects whether qualitatively or quantitatively; just because the water electric dipole is considered explicitly in the model, one can reproduce the correct capacitance behaviors. Once the electric dipole is removed from the model and using the dielectric constant to approximate the electric effect of the water molecule, the resulting capacitance behaviors no longer accord with the experiment behaviors.

This study shows the validity of the dipole dimer hard sphere model in assisting to describe the aqueous EDLC capacitance behaviors. In future research, various parameters

RETRACTED

in the model need to be determined through coordinating relevant experimental data. We will report in subsequent studies.

Author Contributions: Conceptualization, S.Z.; Methodology, S.Z.; Validation, Y.D.; Formal analysis, S.Y. and S.Z.; Investigation, S.Y.; Resources, Y.D.; Writing—original draft, S.Y.; Writing—review & editing, S.Z.; Supervision, S.Z.; Funding acquisition, S.Z. All authors have read and agreed to the published version of the manuscript.

Funding: This research was funded by National Natural Science Foundation of China (Grants 22173117) and High Performance Computing Center of Central South University.

Conflicts of Interest: The authors declare no conflict of interest.

References

1. Simon, P.; Gogotsi, Y. Charge storage mechanism in nanoporous carbons and its consequence for electrical double layer capacitors. *Philos. Trans. R. Soc. A Math. Phys. Eng. Sci.* **2010**, *368*, 3457–3467. [CrossRef] [PubMed]
2. Lethesh, K.C.; Bamgbopa, M.O.; Susantyoko, R.A. Prospects and Design Insights of Neat Ionic Liquids as Supercapacitor Electrolytes. *Front. Energy Res.* **2021**, *9*, 741772. [CrossRef]
3. Schütter, C.; Pohlmann, S.; Balducci, A. Industrial Requirements of Materials for Electrical Double Layer Capacitors: Impact on Current and Future Applications. *Adv. Energy Mater.* **2019**, *9*, 1900334. [CrossRef]
4. Przygocki, P.; Abbas, Q.; Gorska, B.; Beguin, F. High-energy hybrid electrochemical capacitor operating down to-40 degrees C with aqueous redox electrolyte based on choline salts. *J. Power Sources* **2019**, *427*, 283–292. [CrossRef]
5. Gorska, B.; Bujewska, P.; Fic, K. Thiocyanates as attractive redox-active electrolytes for high-energy and environmentally-friendly electrochemical capacitors. *Phys. Chem. Chem. Phys.* **2017**, *19*, 7923–7935. [CrossRef] [PubMed]
6. Poudel, M.B.; Kim, H.J. Confinement of Zn-Mg-Al-layered double hydroxide and α-Fe_2O_3 nanorods on hollow porous carbon nanofibers: A free-standing electrode for solid-state symmetric supercapacitors. *Chem. Eng. J.* **2021**, *429*, 132345. [CrossRef]
7. Poudel, M.B.; Kim, A.R.; Ramakrishan, S.; Logeshwaran, N.; Ramasamy, S.K.; Kim, H.J.; Yoo, D.J. Integrating the essence of metal organic framework-derived ZnCoTe–N–C/MoS_2 cathode and ZnCo-NPS-N-CNT as anode for high-energy density hybrid supercapacitors. *Compos. Part B* **2022**, *247*, 110339. [CrossRef]
8. Martins, V.L.; Mantovi, P.S.; Torresi, R.M. Suppressing early capacitance fade of electrochemical capacitors with water-in-salt electrolytes. *Electrochim. Acta* **2021**, *372*, 137854. [CrossRef]
9. Liu, S.; Klukas, R.; Porada, T.; Furda, K.; Fernández, A.M.; Balducci, A. Potassium formate-based electrolytes for high performance aqueous electrochemical capacitors. *J. Power Sources* **2022**, *541*, 231657. [CrossRef]
10. Yambou, P.; Beguin, F. Effect of salt concentration in aqueous LiTFSI electrolytes on the performance of carbon-based electrochemical capacitors. *Electrochim. Acta* **2021**, *389*, 138687.
11. Messias, A.; da Silva, D.A.C.; Fileti, E.E. Salt-in-water and water-in-salt electrolytes: The effects of the asymmetry in cation and anion valence on their properties. *Phys. Chem. Chem. Phys.* **2021**, *24*, 336–346. [CrossRef]
12. Martins, V.L.; Obana, T.T.; Torresi, R.M. Electroactivity of 3D conducting polymers in water-in-salt electrolyte and their electrochemical capacitor performance. *J. Electroanal. Chem.* **2021**, *880*, 114822. [CrossRef]
13. Lannelongue, P.; Bouchal, R.; Mourad, E.; Bodin, C.; Olarte, M.; le Vot, S.; Favier, F.; Fontaine, O. "Water-in-Salt" for Supercapacitors: A Compromise between Voltage, Power Density, Energy Density and Stability. *J. Electrochem. Soc.* **2018**, *165*, A657–A663. [CrossRef]
14. Li, J.; Yun, X.; Hu, Z.; Xi, L.; Li, N.; Tang, H.; Lu, P.; Zhu, Y. Three-dimensional nitrogen and phosphorus co-doped carbon quantum dots/reduced graphene oxide composite aerogels with a hierarchical porous structure as superior electrode materials for supercapacitors. *J. Mater. Chem. A* **2019**, *7*, 26311–26325. [CrossRef]
15. Bai, Y.; Li, N.; Yang, C.; Wu, X.; Yang, H.; Chen, W.; Li, H.; Zhao, B.; Wang, P.-F.; Han, X. Realizing high-voltage and ultralong-life supercapacitors by a universal interfacial engineering strategy. *J. Power Sources* **2021**, *510*, 230406. [CrossRef]
16. Huang, J.; Peng, Z.; Xiao, Y.; Xu, Y.; Chen, L.; Xiong, Y.; Tan, L.; Yuan, K.; Chen, Y. Hierarchical Nanosheets/Walls Structured Carbon-Coated Porous Vanadium Nitride Anodes Enable Wide-Voltage-Window Aqueous Asymmetric Supercapacitors with High Energy Density. *Adv. Sci.* **2019**, *6*, 1900550. [CrossRef] [PubMed]
17. Ramavath, J.N.; Potham, S.; Ramanujam, K. Energy-Dense Aqueous Carbon/Carbon Supercapacitor with a Wide Voltage Window. *J. Electrochem. Soc.* **2021**, *168*, 070538. [CrossRef]
18. Ghanem, L.G.; Hamza, M.A.; Taha, M.M.; Allam, N.K. Symmetric supercapacitor devices based on pristine g-C_3N_4 mesoporous nanosheets with exceptional stability and wide operating voltage window. *J. Energy Storage* **2022**, *52*, 104850. [CrossRef]
19. Schranger, H.; Barzegar, F.; Abbas, Q. Hybrid electrochemical capacitors in aqueous electrolytes: Challenges and prospects. *Curr. Opin. Electrochem.* **2020**, *21*, 167–174. [CrossRef]
20. Zhou, S.; Lamperski, S. Unusual properties of the electric double layer in an extremely narrow nanotube. A grand canonical Monte Carlo and classical DFT study. *J. Phys. Chem. Solids* **2022**, *161*, 110440. [CrossRef]
21. Zhou, S.; Zhou, R. Influence of ion structure and solvent electric dipole on ultrananoporous supercapacitor: A lattice model study. *Phys. Scr.* **2022**, *97*, 085402. [CrossRef]

REJECTED

22. Zhou, S. On Capacitance and Energy Storage of Supercapacitor with Dielectric Constant Discontinuity. *Nanomaterials* **2022**, *12*, 2534. [CrossRef] [PubMed]
23. Davey, S.B.; Cameron, A.P.; Latham, K.G.; Donne, S.W. Electrical double layer formation on glassy carbon in aqueous solution. *Electrochim. Acta* **2021**, *386*, 138416. [CrossRef]
24. Allagui, A.; Benaoum, H.; Olendski, O. On the Gouy–Chapman–Stern model of the electrical double-layer structure with a generalized Boltzmann factor. *Phys. A Stat. Mech. Appl.* **2021**, *582*, 126252. [CrossRef]
25. Thillaikkarasi, D.; Karthikeyan, S.; Ramesh, R.; Sengodan, P.; Kavitha, D.; Muthubalasubramanian, M. Electrochemical performance of various activated carbon-multi-walled carbon nanotubes symmetric supercapacitor electrodes in aqueous electrolytes. *Carbon Lett.* **2022**, *34*, 1481–1505. [CrossRef]
26. McDaniel, G.; Park, S. Helmholtz Capacitance of Aqueous NaCl Solutions at the Au(100) Electrode from Polarizable and Nonpolarizable Molecular Dynamics Simulations. *J. Phys. Chem. C* **2022**, *126*, 16461–16476. [CrossRef]
27. Zhou, S.; Zhou, R. Ising model study on effects of solvent electric dipole on ultrananoporous supercapacitor. *Chin. J. Phys.* **2021**, *73*, 391–405. [CrossRef]
28. Zhou, S.; Zhou, R.; Tian, C. Impacts of solvent electric dipole and ion valency on energy storage in ultrananoporous supercapacitor: An ising model study. *J. Phys. Chem. Solids* **2021**, *157*, 110188. [CrossRef]
29. Sun, N.; Gersappe, D. Simulation of diffuse-charge capacitance in electric double layer capacitors. *Mod. Phys. Lett. B* **2017**, *31*, 1650431. [CrossRef]
30. Henderson, D.; Silvestre-Alcantara, W.; Kaja, M.; Lamperski, S.; Wu, J.; Bhuiyan, L.B. Structure and capacitance of an electric double layer of an asymmetric valency dimer electrolyte: A comparison of the density functional theory with Monte Carlo simulations. *J. Mol. Liq.* **2017**, *228*, 236–242. [CrossRef]
31. Bossa, G.V.; Caetano, D.L.Z.; de Carvalho, S.J.; Bohinc, K.; May, S. Modeling the camel-to-bell shape transition of the differential capacitance using mean-field theory and Monte Carlo simulations. *Eur. Phys. J. E* **2018**, *41*, 113. [CrossRef] [PubMed]
32. Docampo-Álvarez, B.; Gómez-González, V.; Cabeza, O.; Ivaništšev, V.B.; Gallego, L.J.; Varela, L.M. Molecular dynamics simulations of novel electrolytes based on mixtures of protic and aprotic ionic liquids at the electrochemical interface: Structure and capacitance of the electric double layer. *Electrochim. Acta* **2019**, *305*, 223–231. [CrossRef]
33. Bo, Z.; Li, C.; Yang, H.; Ostrikov, K.; Yan, J.; Cen, K. Design of Supercapacitor Electrodes Using Molecular Dynamics Simulations. *Nano-Micro Lett.* **2018**, *10*, 33. [CrossRef] [PubMed]
34. Bossa, G.V.; Caetano, D.L.; de Carvalho, S.J.; May, S. Differential capacitance of an electrical double layer with asymmetric ion sizes in the presence of hydration interactions. *Electrochim. Acta* **2019**, *321*, 134655. [CrossRef]
35. Li, S.; Zhao, Z.; Liu, X. Electric double layer structure and capacitance of imidazolium-based ionic liquids with FSI− and Tf− anions at graphite electrode by molecular dynamic simulations. *J. Electroanal. Chem.* **2019**, *851*, 113452. [CrossRef]
36. Voroshylova, I.V.; Ers, H.; Docampo-Álvarez, B.; Pikma, P.; Ivaništšev, V.B.; Cordeiro, M.N.D. Hysteresis in the MD Simulations of Differential Capacitance at the Ionic Liquid–Au Interface. *J. Phys. Chem. Lett.* **2020**, *11*, 10408–10413. [CrossRef] [PubMed]
37. da Silva, D.A.C.; Neto, A.J.P.; Pascon, A.M.; Fileti, E.E.; Fonseca, L.R.C.; Zanin, H.G. Combined Density Functional Theory and Molecular Dynamics Simulations To Investigate the Effects of Quantum and Double-Layer Capacitances in Functionalized Graphene as the Electrode Material of Aqueous-Based Supercapacitors. *J. Phys. Chem. C* **2021**, *125*, 5518–5524. [CrossRef]
38. McDaniel, G. Capacitance of Carbon Nanotube/Graphene Composite Electrodes with [BMIM$^+$][BF4$^-$]/Acetonitrile: Fixed Voltage Molecular Dynamics Simulations. *J. Phys. Chem. C* **2022**, *126*, 5822–5837. [CrossRef]
39. Nigam, R.; Kar, K.K. Simulation Study of Electric Double-Layer Capacitance of Ordered Carbon Electrodes. *Langmuir* **2022**, *38*, 12235–12247. [CrossRef] [PubMed]
40. Nishi, N.; Yasui, S.; Hashimoto, A.; Sakka, T. Anion dependence of camel-shape capacitance at the interface between mercury and ionic liquids studied using pendant drop method. *J. Electroanal. Chem.* **2017**, *789*, 108–113. [CrossRef]
41. Lamperski, S.; Bhuiyan, L.B.; Henderson, U. Off-center charge model revisited: Electrical double layer with multivalent cations. *J. Chem. Phys.* **2018**, *149*, 084706. [CrossRef]
42. Lamperski, S.; Bhuiyan, L.B. Entropy formation of an electrical double layer with divalent off-centre charge cations: Monte Carlo studies. *Mol. Phys.* **2021**, *119*, e1918774. [CrossRef]
43. Guerrero-García, G.I. Local inversion of the mean electrostatic potential, maximum charge reversal, and capacitive compactness of concentrated 1:1 salts: The crucial role of the ionic excluded volume and ion correlations. *J. Mol. Liq.* **2022**, *361*, 119566. [CrossRef]
44. Caetano, D.L.Z.; Bossa, G.V.; de Oliveira, V.M.; Brown, M.A.; de Carvalho, S.J.; May, S. Differential capacitance of an electric double layer with asymmetric solvent-mediated interactions: Mean-field theory and Monte Carlo simulations. *Phys. Chem. Chem. Phys.* **2017**, *19*, 23971–23981. [CrossRef] [PubMed]
45. Voroshylova, I.V.; Ers, H.; Koverga, V.; Docampo-Álvarez, B.; Pikma, P.; Ivaništšev, V.B.; Cordeiro, M.N.D. Ionic liquid–metal interface: The origins of capacitance peaks. *Electrochim. Acta* **2021**, *379*, 138148. [CrossRef]
46. Cruz, C.; Lomba, E.; Ciach, A. Capacitance response and concentration fluctuations close to ionic liquid-solvent demixing. *J. Mol. Liq.* **2022**, *346*, 117078. [CrossRef]
47. Lashkari, S.; Pal, R.; Pope, M.A. Ionic Liquid/Non-Ionic Surfactant Mixtures as Versatile, Non-Volatile Electrolytes: Double-Layer Capacitance and Conductivity. *J. Electrochem. Soc.* **2022**, *169*, 040513. [CrossRef]

REJECTED

48. Jildani, S.R.; Keshavarzi, E. Influence of cation shape asymmetry on the interfacial features and capacitance curve of ionic liquids inside the spherical cavity of the porous electrode as an ionic liquid-based supercapacitor. *Electrochim. Acta* **2022**, *426*, 140832. [CrossRef]
49. Wang, Z.; Chen, J.; Li, Y.; Dong, K.; Yu, Y. EDL structure of ionic liquid-MXene-based supercapacitor and hydrogen bond role on the interface: A molecular dynamics simulation investigation. *Phys. Chem. Chem. Phys.* **2022**, *24*, 5903–5913. [CrossRef] [PubMed]
50. Jiménez-Ángeles, F.; Odriozola, G.; Lozada-Cassou, M. Electrolyte distribution around two like-charged rods: Their effective attractive interaction and angular dependent charge reversal. *J. Chem. Phys.* **2006**, *124*, 134902. [CrossRef] [PubMed]
51. Zhou, S. Effective electrostatic forces between two neutral surfaces with surface charge separation: Valence asymmetry and dielectric constant heterogeneity. *Mol. Phys.* **2022**, *120*, e2094296. [CrossRef]
52. Soares, E.D.A.; Vernin, N.S.; Santos, M.S.; Tavares, F.W. Real Electrolyte Solutions in the Functionalized Mean Spherical Approximation: A Density Functional Theory for Simple Electrolyte Solutions. *J. Phys. Chem. B* **2022**, *126*, 6095–6101. [CrossRef] [PubMed]
53. Grimson, M.J.; Rickayzen, G. Forces between surfaces in electrolyte solutions. *Chem. Phys. Lett.* **1982**, *86*, 71–75. [CrossRef]
54. Frink, L.J.D.; van Swol, F. Oscillatory surface forces: A test of the superposition approximation. *J. Chem. Phys.* **1996**, *105*, 2884. [CrossRef]
55. Patra, N. A three-component model on the structure of colloidal solution with size-asymmetric electrolytes. *Mol. Phys.* **2016**, *114*, 2341–2350. [CrossRef]
56. Modak, B.; Patra, C.N.; Ghosh, S.K.; Das, P. Structure of Colloidal Solution in Presence of Mixed Electrolytes: A Solvent Restricted Primitive Model Study. *J. Phys. Chem. B* **2011**, *115*, 12126–12134. [CrossRef] [PubMed]
57. Zhang, L.; Davis, H.T.; White, H.S. Simulations of solvent effects on confined electrolytes. *J. Chem. Phys.* **1993**, *98*, 5793–5799. [CrossRef]
58. Zhou, S. Solvent granularity in the differential electrical capacitance of supercapacitor and mechanism analysis. *Phys. A Stat. Mech. Its Appl.* **2019**, *533*, 121905. [CrossRef]
59. Zhou, S. A statistical mechanics study on relationship between nanopore size and energy storage in supercapacitors. *J. Phys. Chem. Solids* **2021**, *148*, 109705. [CrossRef]
60. Zhou, S. Inter-surface effective electrostatic interactions in the presence of surface charge discreteness and solvent granularity. *Mol. Phys.* **2020**, *118*, e1778807. [CrossRef]
61. Oleksy, A.; Hansen, J.-P. Towards a microscopic theory of wetting by ionic solutions. I. Surface properties of the semi-primitive model. *Mol. Phys.* **2006**, *104*, 2871–2883. [CrossRef]
62. Oleksy, A.; Hansen, J.-P. Microscopic density functional theory of wetting and drying of a solid substrate by an explicit solvent model of ionic solutions. *Mol. Phys.* **2009**, *107*, 2609–2624. [CrossRef]
63. Zhou, S. Mechanism of oscillation of aqueous electrical double layer capacitance: Role of solvent. *J. Mol. Liq.* **2022**, *364*, 119943. [CrossRef]
64. Oleksy, A.; Hansen, J.-P. Wetting and drying scenarios of ionic solutions. *Mol. Phys.* **2011**, *109*, 1275–1288. [CrossRef]
65. Oleksy, A.; Hansen, J.-P. Wetting of a solid substrate by a "civilized" model of ionic solutions. *J. Chem. Phys.* **2010**, *132*, 204702. [CrossRef] [PubMed]
66. Reindl, A.; Bier, M.; Dietrich, S. Electrolyte solutions at curved electrodes. II. Microscopic approach. *J. Chem. Phys.* **2017**, *146*, 154704. [CrossRef] [PubMed]
67. Henderson, D.; Jiang, D.E.; Jin, Z.; Wu, J. Application of Density Functional Theory To Study the Double Layer of an Electrolyte with an Explicit Dimer Model for the Solvent. *J. Phys. Chem. B* **2012**, *116*, 11356–11361. [CrossRef] [PubMed]
68. Yang, K.-L.; Yiacoumi, S.; Tsouris, C. Monte Carlo simulations of electrical double-layer formation in nanopores. *J. Chem. Phys.* **2002**, *117*, 8499–8507. [CrossRef]
69. Jain, S.; Dominik, A.; Chapman, W.G. Modified interfacial statistical associating fluid theory: A perturbation density functional theory for inhomogeneous complex fluids. *J. Chem. Phys.* **2007**, *127*, 244904. [CrossRef] [PubMed]
70. Pernice, M.; Walker, H.F. NITSOL: A Newton Iterative Solver for Nonlinear Systems. *SIAM J. Sci. Comput.* **1998**, *19*, 302–318. [CrossRef]
71. Booth, M.J.; Schlijper, A.; Scales, L.; Haymet, A. Efficient solution of liquid state integral equations using the Newton-GMRES algorithm. *Comput. Phys. Commun.* **1999**, *119*, 122–134. [CrossRef]
72. Lu, B.; Cheng, X.; McCammon, J.A. "New-version-fast-multipole-method" accelerated electrostatic calculations in biomolecular systems. *J. Comput. Phys.* **2007**, *226*, 1348–1366. [CrossRef] [PubMed]
73. Averkin, N.; Gatsonis, N.A. A parallel electrostatic Particle-in-Cell method on unstructured tetrahedral grids for large-scale bounded collisionless plasma simulations. *J. Comput. Phys.* **2018**, *363*, 178–199. [CrossRef]
74. Nguyen, T.; Li, H.; Bagchi, D.; Solis, F.J.; de la Cruz, M.O. Incorporating surface polarization effects into large-scale coarse-grained Molecular Dynamics simulation. *Comput. Phys. Commun.* **2019**, *241*, 80–91. [CrossRef]
75. Bi, S.; Li, Z.; Xiao, D.; Li, Z.; Mo, T.; Feng, G.; Zhang, X. Pore-Size-Dependent Capacitance and Charging Dynamics of Nanoporous Carbons in Aqueous Electrolytes. *J. Phys. Chem. C* **2022**, *126*, 6854–6862. [CrossRef]
76. Heo, M.; Shin, G.R.; Kim, S.-C. Differential capacitance of uniformly charged hard-sphere ions in planar electric double layers. *J. Stat. Mech. Theory Exp.* **2019**, *2019*, 083207. [CrossRef]

RETRACTED

77. Zhang, Y.; Cummings, P.T. Effects of Solvent Concentration on the Performance of Ionic-Liquid/Carbon Supercapacitors. *ACS Appl. Mater. Interfaces* **2019**, *11*, 42680–42689. [CrossRef]
78. Kłos, J.; Lamperski, S. Monte Carlo study of molten salt with charge asymmetry near the electrode surface. *J. Chem. Phys.* **2014**, *140*, 054703. [CrossRef]
79. Khademi, M.; Barz, D.P.J. Structure of the Electrical Double Layer Revisited: Electrode Capacitance in Aqueous Solutions. *Langmuir* **2020**, *36*, 4250–4260. [CrossRef]
80. Watzele, S.A.; Katzenmeier, L.; Sabawa, J.P.; Garlyyev, B.; Bandarenka, A.S. Temperature dependences of the double layer capacitance of some solid/liquid and solid/solid electrified interfaces. An experimental study. *Electrochim. Acta* **2021**, *391*, 138969. [CrossRef]
81. Boda, D.; Henderson, D.; Chan, K.-Y.; Wasan, D.T. Low temperature anomalies in the properties of the electrochemical interface. *Chem. Phys. Lett.* **1999**, *308*, 473–478. [CrossRef]
82. Olivieri, J.-F.; Hynes, J.T.; Laage, D. Confined Water's Dielectric Constant Reduction Is Due to the Surrounding Low Dielectric Media and Not to Interfacial Molecular Ordering. *J. Phys. Chem. Lett.* **2021**, *12*, 4319–4326. [CrossRef] [PubMed]
83. Murota, K.; Saito, T. Pore Size Effects on Surface Charges and Interfacial Electrostatics of Mesoporous Silicas. *Phys. Chem. Chem. Phys.* **2022**, *24*, 18073–18082. [CrossRef] [PubMed]
84. Zhou, S. Capacitance of electrical double layer formed inside a single infinitely long cylindrical pore. *J. Stat. Mech. Theory Exp.* **2018**, *2018*, 103203. [CrossRef]

Disclaimer/Publisher's Note: The statements, opinions and data contained in all publications are solely those of the individual author(s) and contributor(s) and not of MDPI and/or the editor(s). MDPI and/or the editor(s) disclaim responsibility for any injury to people or property resulting from any ideas, methods, instructions or products referred to in the content.

RETRACTED